Pergamon

Int. J. Heat Mass Transfer. Vol. 38, No. 16, pp. 3053–3063, 1995

0017-9310/95 $9.50+0.00

0017-9310(95)00049-6

Heat transfer and fluid flow characteristics of plate-array aligned at angles to the flow direction

L. B. WANG and W. Q. TAO†

School of Energy and Power Engineering, Xi'an Jiaotong University, Xi'an, Shaanxi 710049, China

(*Received* 13 *December* 1994)

Abstract—The periodically fully developed laminar heat transfer and fluid flow characteristics of an array of uniform plate length, aligned at angles to the air flow direction have been investigated numerically in the range Re = 50–2300 using body-fitted coordinate system. Multisurface transformation is used in the grid generation in order to retain the periodic corresponding relations of the surfaces or lines in both physical and computational spaces. The computed results exhibit good agreement with the experimental data available in the literature. The results also show that both the intensity of heat transfer and the pressure drop increase with the increases in oblique angle and plate length.

INTRODUCTION

Flow interruption at periodic intervals is a well-known technique for enhancing heat transfer, and the louvered fin and off-set fin surfaces are examples of its applications, which have been widely used in automobiles, chemical engineering, refrigerators, etc. Numerous experimental and numerical studies have been carried out on heat transfer and fluid flow characteristics for such kinds of configurations. It has been found experimentally that after passing several cycles, typically 3–5, the fluid flow and heat transfer become periodically fully developed [1–5]. A knowledge of fluid flow and heat transfer in the fully developed region is required in the design and performance evaluation for most of the engineering applications.

Sparrow *et al.* [6, 7] and Patankar *et al.* [8] assumed the plate thickness to be negligible and obtained numerical solutions for laminar flow and heat transfer for the interrupted plates sit in the flow field. Patankar and Prakash [9] analysed the effect of plate thickness on the laminar flow and heat transfer in interrupted-plate passages. In all these plate arrangements, the boundaries of the solid plates were aligned with the Cartesian coordinates, therefore the discretization of the computation domain could be conducted easily. As for the cases where boundaries of the solid plates are not aligned with the Cartesian coordinates, the numerical analysis becomes more complicated in generating an appropriate grid system.

Asako and Faghri [10] carried out a numerical prediction for an array of interrupted plates positioned obliquely to the flow direction, with an algebraic coordinate transformation technique to map the irregular solution domain onto a rectangle, the thickness of plate being neglected. Pang *et al.* [11] performed numerical investigations on an array of interrupted plates positioned convergently–divergently along the flow direction in the Cartesian coordinates using the blocking-off technique and the stepwise succession to simulate the plate boundary.

The purpose of the present study is to carry out a numerical analysis of the heat transfer and fluid flow characteristics of arrays with uniform plate length aligned at angles to the flow direction in a body-fitted coordinate system, to examine the feasibility of the mutual replacement technique for treating the periodic boundary conditions in just one-cycle domain in the computational space, and to perform a parametric study of the effects of the Reynolds number, the oblique angle, θ, and the ratio of plate length to transverse space between plates, L/T_p, on the pressure drop and heat transfer for the arrays that have been experimentally studied by Zhang and Lang [3]. The numerical prediction will be compared with experimental results so to make a general evaluation of the grid generation analysis technique adopted in this paper.

PHYSICAL MODEL AND MATHEMATICAL FORMULATION

The problem to be analysed is schematically shown in Fig. 1, an array of uniform length is positioned obliquely to the flow direction. The engineering background of this study is the heat transfer and fluid flow in louvered fins used in automobile and other motor vehicle radiators, where the fins are formed by slitting a continuous thin copper plate and then turning the slitted segments at an angle. In this case, $L_p = L$. The geometric parameters of array studied are copied from Zhang and Lang [3], as listed in Table 1.

The analysis is based on the following assumptions: (1) the fluid properties are constant; (2) the flow and

†Author to whom correspondence should be addressed.

NOMENCLATURE

c_p	specific heat of constant pressure
f	pressure drop factor
h_x	local heat transfer coefficient [W m^{-2} °C^{-1}]
J	Jacobean of coordinate transformation
L	plate length [m]
M_r	relative maximum mass flow rate unbalance in one control volume
Nu	Nusselt number
p	pressure, P_a
Pr	Prandtl number
q_x	local heat flux [W m^{-2}]
Re	Reynolds number
T	temperature [°C]
T_p	transverse spacing between two adjacent plates [m]
T_b	bulk temperature [°C]
T_w	wall temperature [°C]
u_i	velocity components in Cartesian coordinates [m s^{-1}]
U, V	contravariant velocity components in ξ and η direction [m s^{-1}]
x	distance from leading point along the plate surface [m]
x_i	Cartesian coordinates [m].

Greek symbols

α, β, γ	metric coefficients
δ	thickness of plate [m]
θ	oblique angle, degree
Θ	dimensionless temperature
λ	thermal conductivity [W m^{-1} °C^{-1}]
μ	fluid dynamic viscosity [kg m^{-1} s^{-1}]
ξ, η	coordinates in transformed plane
ρ	fluid density [kg m^{-3}]
ϕ	general dependent variable.

Subscripts

m	mean
ξ, η	partial derivatives with respect to ξ and η.

Superscripts

*	value of the previous iteration.

heat transfer are in steady state, laminar and periodically fully developed; (3) the body force and the dissipation term are neglected. The computation domain is chosen as in Fig. 1(b). The fluid flow and heat transfer can be specified by the following equations with Cartesian tensor notation:

continuity equation

$$\frac{\partial}{\partial x_i}(\rho u_i) = 0 \tag{1}$$

momentum equations

$$\frac{\partial}{\partial x_i}(\rho u_i u_k) = \frac{\partial}{\partial x_i}\left(\mu \frac{\partial u_k}{\partial x_i}\right) - \frac{\partial p}{\partial x_k}, \quad k = 1, 2 \tag{2}$$

energy equation

$$\frac{\partial}{\partial x_i}(\rho c_p u_i T) = \frac{\partial}{\partial x_i}\left(\lambda \frac{\partial T}{\partial x_i}\right) \tag{3}$$

boundary conditions:

$$\begin{aligned} u(x,y)|_{AE} &= u(x,y)|_{DH} \\ v(x,y)|_{AE} &= v(x,y)|_{DH} \\ \Theta(x,y)|_{AE} &= \Theta(x,y)|_{DH} \end{aligned} \tag{4}$$

$$\begin{aligned} u(x,y)|_{BC} &= u(x,y)|_{FG} \\ v(x,y)|_{BC} &= v(x,y)|_{FG} \\ T(x,y)|_{BC} &= T(x,y)|_{FG}. \end{aligned} \tag{5}$$

In addition, the following conditions must be satisfied at the surfaces of the solid plates

$$\begin{aligned} u(x,y) &= 0 \\ v(x,y) &= 0 \\ T(x,y) &= T_w. \end{aligned} \tag{6}$$

The dimensionless temperature in equation (4) is defined as:

$$\Theta(x,y) = (T(x,y) - T_w)/(T_b(x) - T_w). \tag{7}$$

Attention is turned to coordinate transformation and grid generation. The continuity equation and the conservation form of the transport equation for a general dependent variable in a generalized coordinate system (ξ, η) can be written as follows:

$$\frac{\partial}{\partial \xi}(\rho U) + \frac{\partial}{\partial \eta}(\rho V) = 0 \tag{8}$$

$$\frac{\partial}{\partial \xi}(\rho U \phi) + \frac{\partial}{\partial \eta}(\rho V \phi) = \frac{\partial}{\partial \xi}\left[\frac{\Gamma_\phi}{J}\left(\alpha \frac{\partial \phi}{\partial \xi} - \beta \frac{\partial \phi}{\partial \eta}\right)\right] + \frac{\partial}{\partial \eta}\left[\frac{\Gamma_\phi}{J}\left(-\beta \frac{\partial \phi}{\partial \xi} + \gamma \frac{\partial \phi}{\partial \eta}\right)\right] + JS_\phi \tag{9}$$

where S_ϕ is the source term in computational space and the contravariant velocities U, V and the geometric parameters are given as

$$U = uy_\eta - vx_\eta, \quad V = vx_\xi - uy_\xi \tag{10}$$

$$J = x_\xi y_\eta - x_\eta y_\xi, \quad \beta = x_\xi x_\eta + y_\xi y_\eta \tag{11}$$

$$\alpha = x_\eta^2 + y_\eta^2, \quad \gamma = x_\xi^2 + y_\xi^2. \tag{12}$$

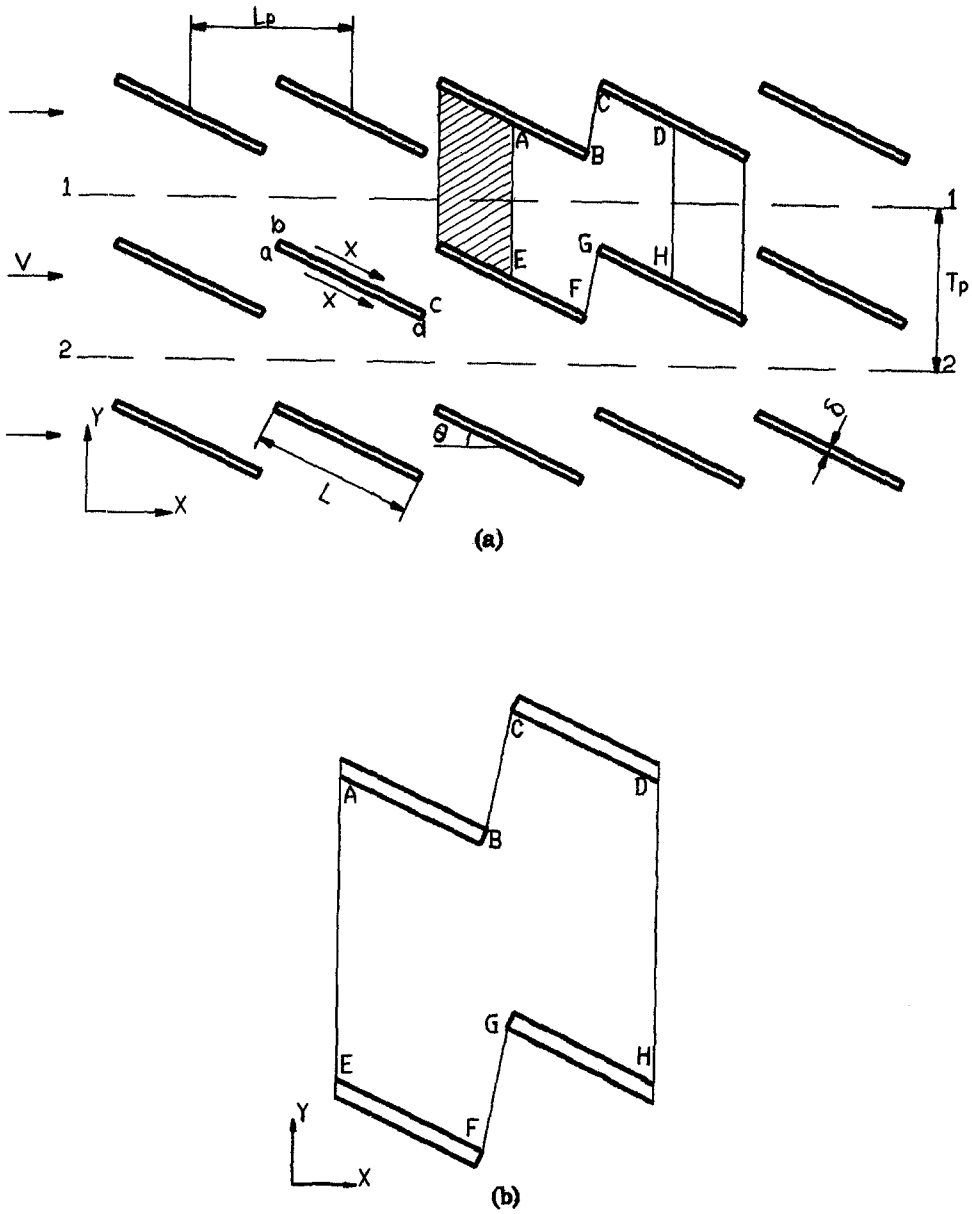

Fig. 1. Schematic diagram of the configuration studied: (a) interrupted plate array; (b) computation domain.

Table 1. Geometric parameters (δ = 1.5 mm, T_p = 30 mm)

Case	θ (degree)	L_p (mm)	L (mm)
1	10	30	30
2	15	30	30
3	20	30	30
4	25	30	30
5	30	30	30
6	35	30	30
7	25	37.5	37.5
8	25	22.5	22.5

The corresponding grid generation scheme used is the multisurface transformation [13], of which the details can be found in references [13, 14].

A typical grid system generated by this method is shown in Fig. 2. It should be noted that the sharp corners of the domain in physical space are not approximated with smooth curves to prevent singularities as was done in Asako and Faghri [10]. To prevent the singularities at the sharp corners special care was taken in calculating the geometrical derivatives such as x_ξ and y_ξ, such that the values of x_ξ and y_ξ at the points near the corner were calculated by the backward or forward difference according to the point

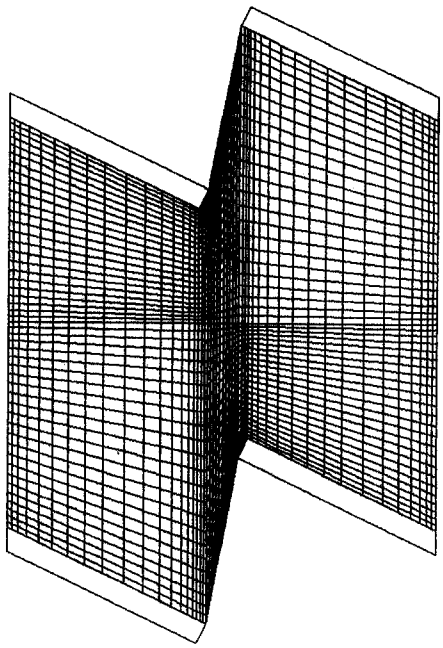

Fig. 2. Typical grid mesh used in computation.

position relative to the corner, and the derivatives of x_ξ, y_ξ at the corner points were calculated according to the derivatives of the points situated aside the corner points. The simple arithmetic mean was used here.

NUMERICAL PROCEDURE

The discretization of the transport equations in the computational domain was performed on a staggered grid by using the finite-volume approach. A SIMPLE-like solution algorithm in the computational domain was adopted to deal with the linkage between pressure and velocities, the details of which may be found in Shyy [15] and Tao [16]. Because the grid is non-orthogonal, the pressure correction equations contain cross derivatives, which lead to a nine-point formulation. In this study the cross derivatives were incorporated into the source term, and a five-point solver was used to solve the algebraic equations.

Attention should be paid to the implementation of the periodic boundary conditions in the computational domain. Since the solution domain is exactly one cycle, the adoption of the mutual replacement method as conducted by Amano *et al.* [17] and Xin and Tao [18] needs some special treatment. In this paper, the following linear interpolation was used for the implementation of the periodic boundary conditions in the η direction:

$$\phi(i,1) = \phi(i,M_1) = (\phi^*(i,2)+\phi^*(i,M_2))/2 \quad (i_F \leqslant i \leqslant i_G) \quad (13)$$

where '*' represents the previous iteration, and M_1, M_2 are the last and last but one indices in the η direction. This implies that after each iteration, the arithmetic mean value of $\phi(i,2)$ and $\phi(i,M_2)$ is assigned to the top and bottom boundaries and serves as the boundary condition for the next iteration.

The following linear interpolation was used for the implementation of the periodic boundary conditions in the ξ direction:

$$\phi(\xi_{A\text{-}E},\eta) = \phi(\xi_{D\text{-}H},\eta) = (\phi^*(\xi_{1\text{-}1},\eta)+\phi^*(\xi_{2\text{-}2},\eta))/2.0 \quad (14)$$

where $\xi_{1\text{-}1}$ and $\xi_{2\text{-}2}$ are positions corresponding to the lines 1-1 and 2-2 in Fig. 3. As far as the temperature is concerned, the periodic condition is valid only for the dimensionless value. Thus, the dimensionless temperatures at the cycle inlet and outlet for next iteration were taken as the interpolation values determined below,

$$\Theta = \tfrac{1}{2}\left(\frac{T(\xi_{1\text{-}1},\eta)-T_w}{T_b(\xi_{1\text{-}1})-T_w}+\frac{T(\xi_{2\text{-}2},\eta)-T_w}{T_b(\xi_{2\text{-}2})-T_w}\right). \quad (15)$$

The local temperatures at the cycle inlet and outlet were calculated, respectively, by

$$T(\xi_{AE},\eta) = T_w+\Theta[T_b(\xi_{AE})-T_w] \quad (16)$$

$$T(\xi_{DH},\eta) = T_w+\Theta[T_b(\xi_{DH})-T_w]. \quad (17)$$

The local heat transfer coefficient was determined by

$$h_x = \frac{q_x}{(T_b(\xi_{DH})-T_b(\xi_{AE}))/(\ln(T_w-T_b(\xi_{AE}))-\ln(T_w-T_b(\xi_{DH})))}. \quad (18)$$

The bulk temperature $T_b(\xi)$ was defined as

$$T_b = \int_{\eta_1}^{\eta_{M_1}} T(\xi,\eta)u(\xi,\eta)\sqrt{\alpha}\,d\eta \Big/ \int_{\eta_1}^{\eta_{M_1}} u(\xi,\eta)\sqrt{\alpha}\,d\eta \quad (19)$$

while the local heat flux was computed by Fourier's law of heat conduction. The value of heat flux at the plate surface was determined by

$$q_{n_1} = -\lambda\frac{\gamma T_\eta-\beta T_\xi}{J\sqrt{\gamma}}\bigg|_{\eta=\eta_1}, \qquad q_{n_2} = -\lambda\frac{\gamma T_\eta-\beta T_\xi}{J\sqrt{\gamma}}\bigg|_{\eta=\eta_{M_1}}. \quad (20)$$

The average heat flux of the plate surface was therefore determined by

$$q_m = \frac{\int_{\xi_E}^{\xi_F} q_{n_1}\sqrt{\gamma}\,d\xi+\int_{\xi_G}^{\xi_H} q_{n_1}\sqrt{\gamma}\,d\xi+\int_{\xi_A}^{\xi_B} q_{n_2}\sqrt{\gamma}\,d\xi+\int_{\xi_C}^{\xi_D} q_{n_2}\sqrt{\gamma}\,d\xi}{\int_{\xi_E}^{\xi_F}\sqrt{\gamma}\,d\xi+\int_{\xi_G}^{\xi_H}\sqrt{\gamma}\,d\xi+\int_{\xi_A}^{\xi_B}\sqrt{\gamma}\,d\xi+\int_{\xi_C}^{\xi_D}\sqrt{\gamma}\,d\xi}. \quad (21)$$

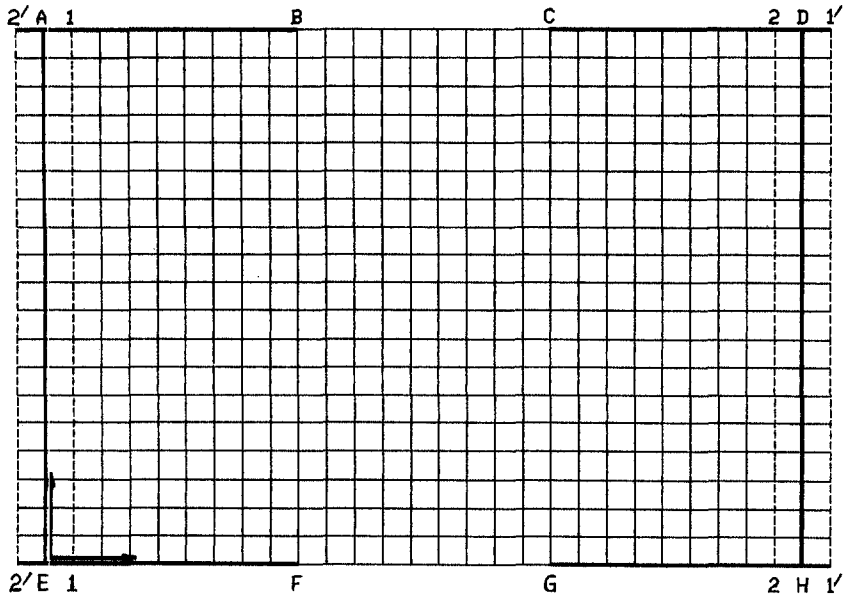

Fig. 3. Computation domain with virtual cells.

Then, the plate-average heat transfer coefficient of one cycle was computed by

$$h_m = q_m/\{[T_b(\xi_{DH}) - T_b(\xi_{AE})]/ [\ln[T_w - T_b(\xi_{AE})] - \ln[T_w - T_b(\xi_{DH})]]\}. \quad (22)$$

The Reynolds number and the plate-average Nusselt number were defined as

$$Re = \rho u_m L/\mu \quad Nu = h_m L/\lambda. \quad (23)$$

The per-plate pressure drop factor of one cycle was determined as

$$f = [p_m(\xi_{AE}) - p_m(\xi_{DH})]/(\rho u_m^2/2). \quad (24)$$

The velocity field convergence criterion used in this study was that the maximum relative mass flow rate unbalance in one control volume, M_r, was less than 10^{-5}. The value of M_r is calculated by

$$M_r = \text{MAX}(|b|)/\int_{\eta_1}^{\eta_M} \rho U(\xi_{AE}, \eta)\, d\eta \quad (25)$$

where b is the residual of mass flow rate for a control volume in the computational domain. U is the contravariant velocity. The number of iterations needed to obtain a converged velocity field is usually less than 2500.

A preliminary computation was performed on two grid-systems (40×39, 57×45) to assure the grid independence of the numerical solution for the case $L = 30$ mm, $L/T_p = 1$, $Re = 500$. The difference between the two solutions of Nu was 1.3% and that of f was 0.5% (see Table 2).

Table 2. Grid independence study ($L = 30$ mm, $\theta = 35°$, $L/T_p = 1$, $Re = 500$)

Grid size	Nu	f
40×39	20.6656	2.4087
57×45	20.9430	2.4213

RESULTS AND DISCUSSION

Flow field

The typical predicted velocity field is shown in Fig. 4. The configuration of $L/T_p = 1$, and $\theta = 25°$ (Case 4) is commonly used in engineering applications. The velocity fields plotted in Fig. 5 show how the flow pattern changes with increasing θ at the same Reynolds number (1500), while in Fig. 6, the effect of L/T_p at $\theta = 25°$ and $Re = 1500$ is presented. It is better to imagine that the right-hand part of the computation domain, CDHG in Fig. 1(b) has been moved to the shaded area of Fig. 1(a), so that a complete cycle of the plate array can be formed, just like the left part of Fig. 4(b). Hence, the characteristics of flow fields shown in Figs. 4–6 may be summarized as follows. First, the velocity is approximately one-dimensional on line 1-1 in Fig. 1(a), which is a center-line or more exactly a pseudo-center-line. Secondly, there are two recirculating flows in a one-cycle flow field, one located in the top-left region and the other one located in the bottom-right corner. This is quite reasonable. The upper half of one-cycle in Fig. 4(b), that is, the flow region that is located over the line 1-1 is that of a convergent two-dimensional nozzle, for which the recirculating zone is usually located in the inlet region of the nozzle, while the lower half is just that of a

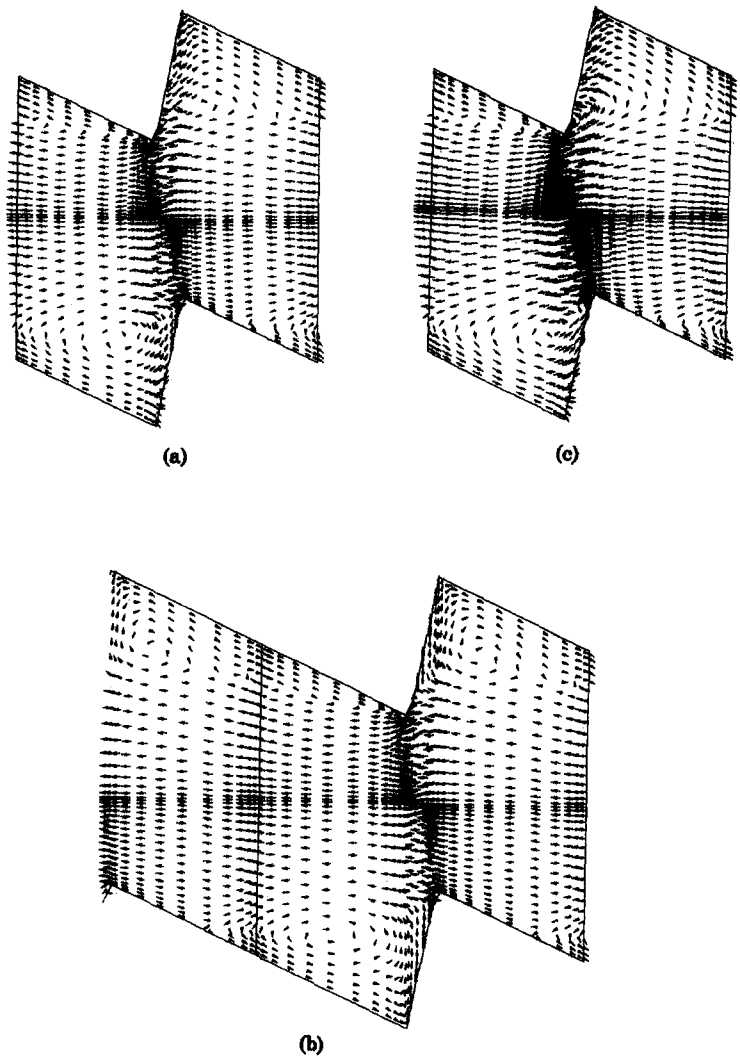

Fig. 4. Flow patterns at different Reynolds numbers ($L/T_p = 1$, $\Theta = 25°$): (a) $Re = 500$; (b) $Re = 1000$; (c) $Re = 2300$.

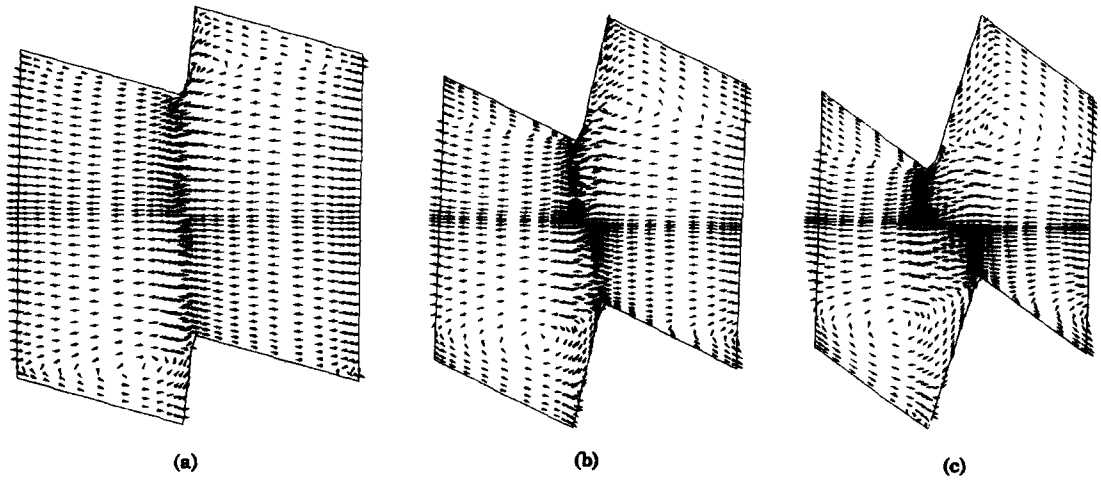

Fig. 5. Flow patterns at different angles ($L/T_p = 1$, $Re = 1500$): (a) $\Theta = 15°$; (b) $\Theta = 25°$; (c) $\Theta = 35°$.

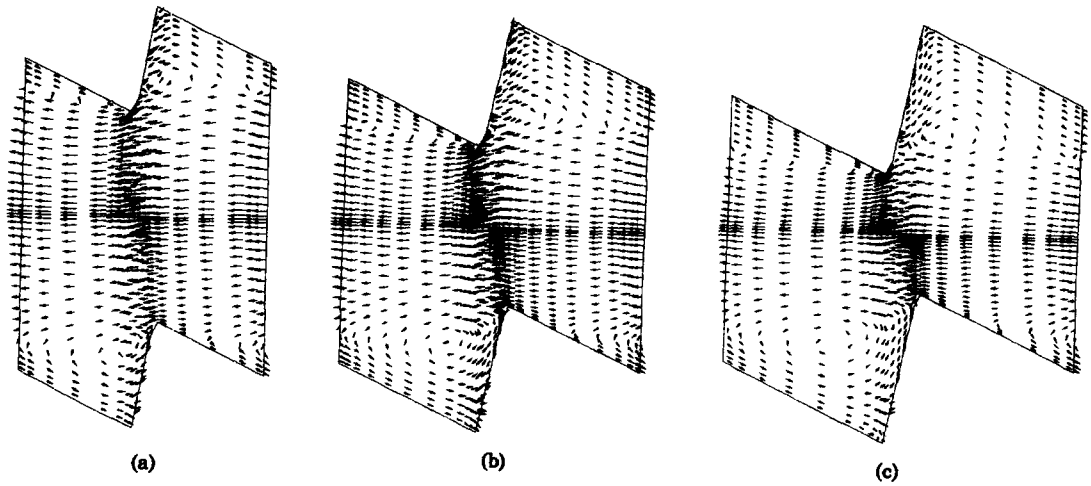

Fig. 6. Flow patterns at different L/T_p($Re = 1500$, $\Theta = 25°$): (a) $L/T_p = 0.75$; (b) $L/T_p = 1.0$; (c) $L/T_p = 1.25$

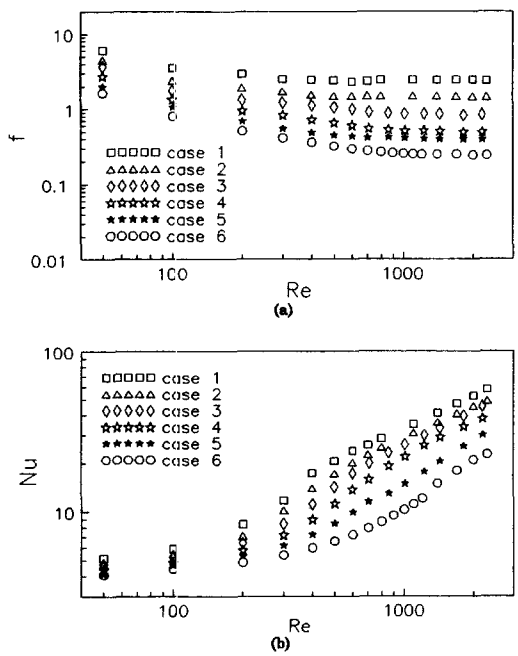

Fig. 7. Numerically predicted pressure drop factor and Nusselt number for different oblique angle: (a) f vs Re; (b) Nu vs Re.

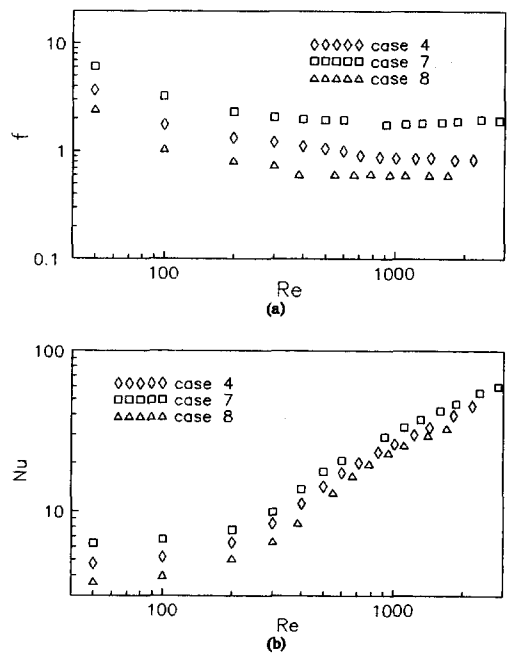

Fig. 8. Numerically predicted pressure factors and Nusselt numbers for different L/T_p: (a) f vs Re; (b) Nu vs Re.

divergent nozzle, for which a recirculating flow is expected to occur near the exit of the nozzle. Third, it can be seen from the figures that, with increasing Reynolds number, attack angle and L/T_p, the sizes of the two recirculating zones increase. This variation will surely affect both the pressure-drop factor and the plate-average Nusselt number.

Pressure drop factor, f

The calculated pressure drop factors for different configurations, listed in Table 1, are shown in Figs. 7(a) and 8(a). From these results, the following features may be noted. First, in the low Reynolds number region (approximately less than 100), the variation of f with Re has the same trend as that of a fully developed laminar flow in a continuous duct, i.e. f decreases with the increase in Reynolds number. This is the flow region where the pressure drop is mainly caused by the surface friction effect. The form drag of the plate (including the inlet and outlet effects) gradually becomes significant with further increase in Reynolds number, and finally, it becomes predominant, leading to a constant value of f for each case. Secondly, the higher the angle θ, the larger the value of f in the entire range of Reynolds number studied. This implies that even at very low Reynolds number (about 50), the form drag of the plate still has some effect on the total pressure drop of the cycle. Thirdly, for a given L/T_p,

the starting Reynolds number beyond which the value of f becomes constant is dependent on Re. For $\theta = 35°$, this Reynolds number is about 300, while for $\theta = 10°$, it increases to about 1000. Fourthly, at the same θ and T_p, the increase in L leads to an increase in both the friction effect and the plate form drag, thus the per-plate pressure drop factor increases.

Average heat transfer

The average heat transfer results are presented in Fig. 7(b) and Fig. 8(b) in terms of the plate-average Nusselt number. It can be seen that, in the low Reynolds number region ($Re \leqslant 100$), the plate-average Nusselt number almost remains constant, showing the character of fully developed laminar heat transfer in a continuous duct. This was also revealed by Asako and Faghri [10] and by Pang *et al.* [11]. As $Re > 100$, the increase in Reynolds number leads to an appreciable increase in Nusselt number. For the case $L/T_p = 1$, in the entire range of Reynolds number studied, the larger the angle θ, the higher the plate-average Nusselt number. However, in the low Reynolds number region, the ratio of Nu for $\theta = 35°$ and for $\theta = 10°$ is much less than that in the high Reynolds number region (about 1.3 vs 3.0), indicating the strong effect of the recirculating flow on heat transfer enhancement. On the other hand, for the case $\theta = 25°$ the ratio of Nusselt numbers for $L/T_p = 1.25$ and for $L/T_p = 0.75$ is somewhat larger than that in the higher Reynolds number region (about 2.0 to 1.5). This implies that in the high Reynolds number region, the plate-average heat transfer coefficient for a short plate is actually larger than that of a long plate, since the characteristic length of the long plate is about 1.67 times that of the short plate.

Local heat transfer coefficients

The local heat transfer coefficients of the windward and leeward surfaces are shown in Fig. 9 for case 4 at two Reynolds numbers, and in Fig. 10 the results for cases 1, 3 and 6 at $Re = 1000$ are presented. Here the leeward surface consists of the ab and bc segments in Fig. 1(a) and the windward side of the plate consists of ad and dc. The x coordinate in Figs. 9 and 10 is a local one along the plate surface, for both the windward and leeward sides. It can be found that for the leeward surface, the local heat transfer coefficient has a very significant increase with x in the start region, and reaches its maximum at the point where a boundary layer flow along the plate surface begins. It then rapidly decreases to a quite uniform value in a region about half of the plate length. This is because the boundary layer does not last long downward over the plate surface, rather it meets a counter-direction stream on the surface, mixes with it and then deviates from the surface. The effect of the bottom-right recirculating flow is to cause an increase in the local heat transfer coefficients. At the very end of the leeward surface, the local heat transfer again reaches a maximum, basically because of the rushing-out effect

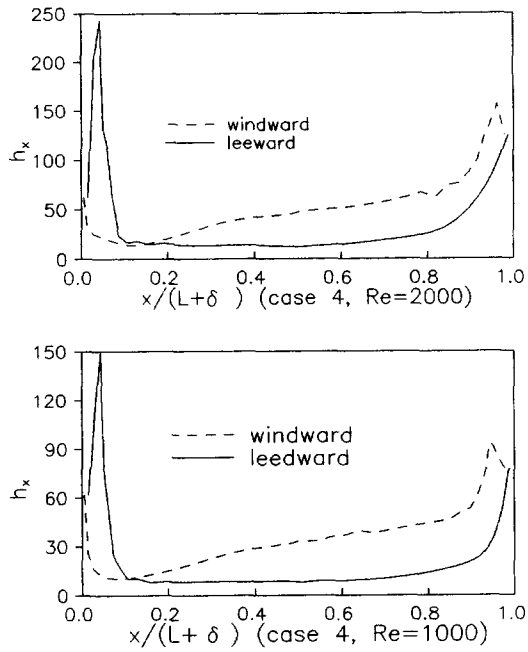

Fig. 9. Local heat transfer coefficient distributions for case 4.

of the fluid flow. As for the windward surface, the local heat transfer coefficient increases principally with the distance from the leading edge, due to the velocity acceleration effect occurring over the obliquely positioned plate. In the region adjacent to the end of the windward surface it has the same variation pattern as in the start region of the leeward surface.

The above-stated overall variation patterns of the local heat transfer coefficients for the windward and leeward surfaces hold for all the cases studied, with some differences mainly in the quantitative level. As expected, the increase in the Reynolds number or oblique angle leads to an increase in the local heat transfer coefficient.

Comparison with experimental results

The computed results for different cases are compared with the results of experiments made by Zhang and Lang [3], as shown in Figs. 11–13. Generally, most of the numerical results agree well with the experimental ones. However, it can be seen from Figs. 11 and 12 that the discrepancy between the numerical and experimental results gradually becomes larger with the decrease in the oblique angle θ. This may be attributed to the local skewness of the grid network generated. As seen from Figs. 1(b) and 2, in the regions of ABEF and CDHG, the generated grid network is approximately orthogonal, while in the region BCGF, the network has rather high non-orthogonality, and so, the smaller the angle θ, the more severe the non-orthogonality of the network, thus leading to an increasing numerical error. However, as far as the pressure drop factor of Case 8 (Fig. 13) is concerned, the discrepancy is up to 30–40%, yet the agreement for Case 8 between the predicted Nusselt number and

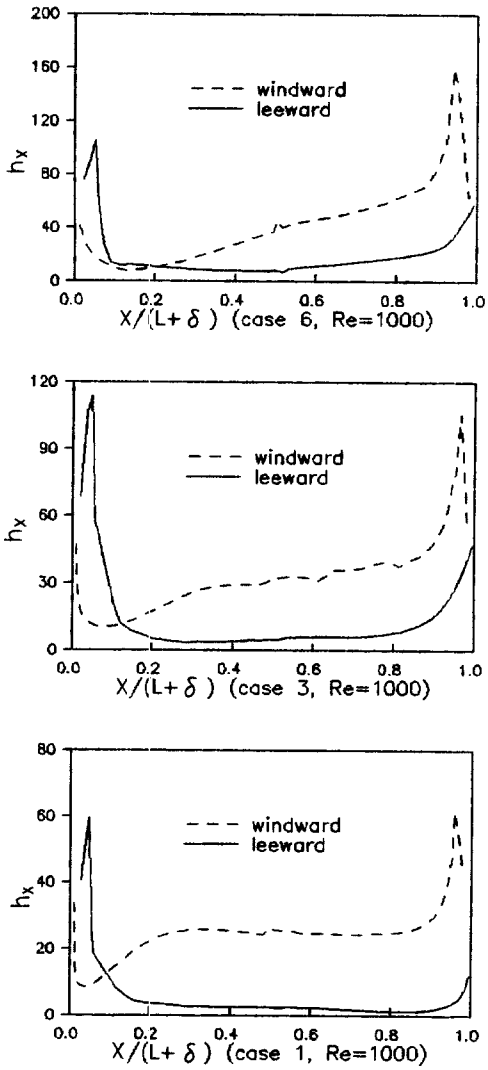

Fig. 10. Local heat transfer coefficient distribution for different oblique angles.

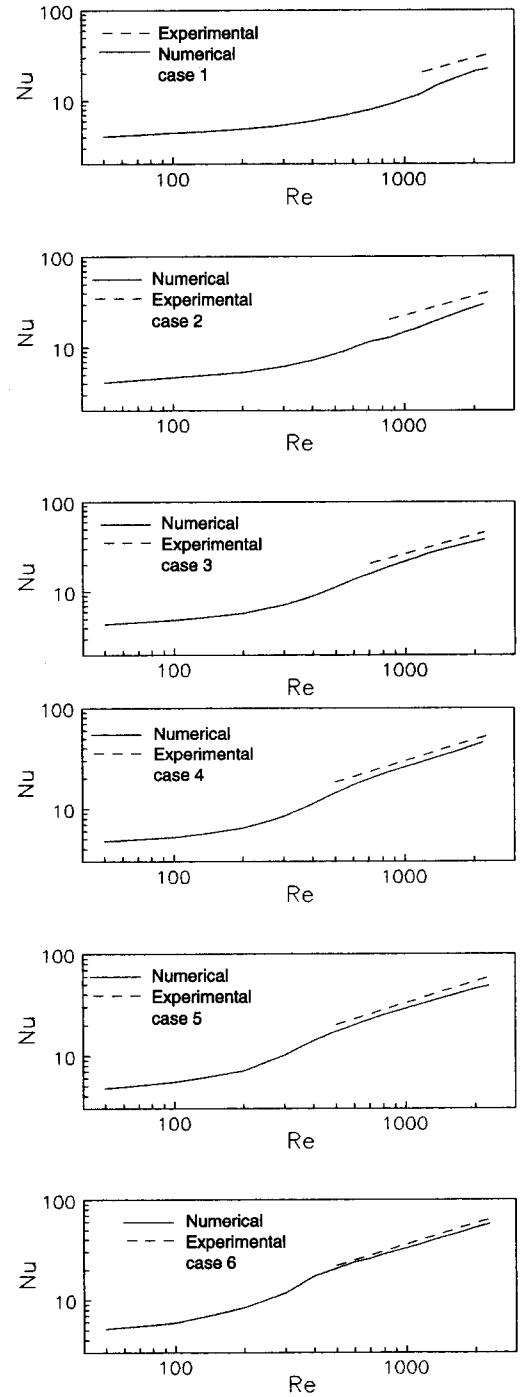

Fig. 11. Comparison of predicted Nusselt number with experimental results for cases 1–6.

the experimental one is quite good; it is the authors' consideration that measurement uncertainty may also play a role.

CONCLUDING REMARKS

A parametric investigation on the fluid flow and heat transfer characteristics of periodically fully developed flows in arrays with uniform plate length and oblique angles to the flow direction has been performed numerically by using the multisurface transformation in the generation of the grid system. The following conclusions can be drawn.

1. The grid networks generated by the multisurface transformation are appropriate, as witnessed by the good agreement between the predicted and measured results. However, for the cases of small oblique angles θ (say, less than 15°), the severe skewness of the generated grid network in the inter-plate region may cause a larger numerical error.

2. The mutual replacement method and the related interpolation technique proposed for implementing the periodic boundary condition in the exactly-one-cycle domain has been successfully extended to the computational space.

3. There are two recirculating zones in one cycle, the top-left region and in the bottom-right region.

However, at the pseudo-center-line, the flow is one-dimensional with the velocity component normal to the line being very small.

4. Both the pressure drop factor and the Nusselt number increase with increases in the Reynolds number (beyond 100), the oblique angle and the ratio of L/T_p. This may be attributed to the enlargement of the two recirculating zones. However, when the Reynolds number exceeds a certain value, the per-cycle pressure drop factor ceases to change with the Reynolds number.

5. In the very low Reynolds number region ($Re \leqslant 100$), the fluid flow and heat transfer within the array behave as an internal laminar flow, characterized by the insensitivity of the Nusselt number to Re and the nearly inverse proportionality of the pressure drop factor to Re.

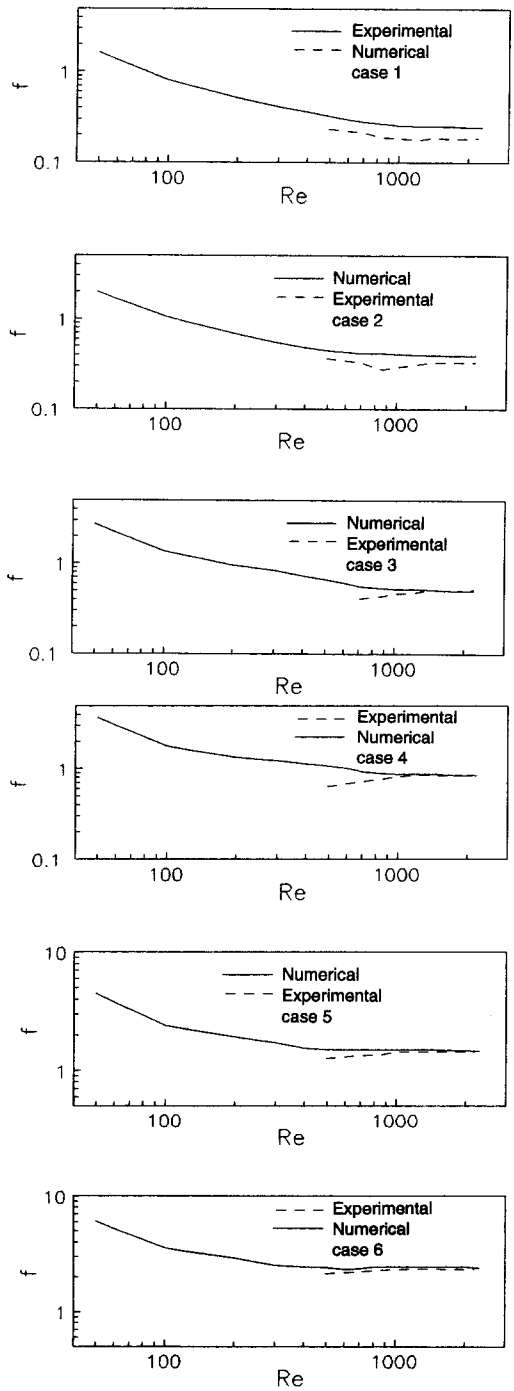

Fig. 12. Comparison of predicted pressure drop factor with experimental results for cases 1–6.

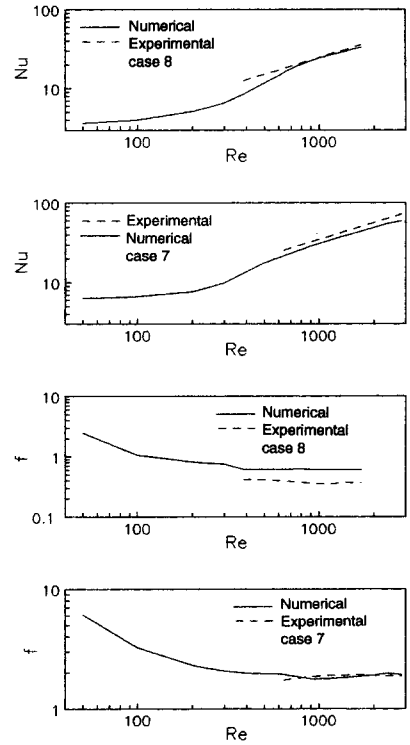

Fig. 13. Comparison of predicted results with experimental ones for cases 7 and 8.

REFERENCES

1. X. J. Yan, H. H. Zhang and W. Q. Tao, An experimental investigation of heat transfer and pressure drop performance for arrays of staggered plates aligned with air flows, *Proceedings of the Eighth International Heat Transfer Conference*, San Francisco, CA, Vol. 4, pp. 2887–2896 (1986).
2. Y. N. Lee, Heat transfer and pressure drop characteristics of an array of plates aligned at angles to the flow in a rectangle duct, *Int. J. Heat Mass Transfer* **29**, 1553–1563 (1986).
3. H. H. Zhang and X. S. Lang, The experimental investigation of oblique angles and interrupted plate lengths for louvered fins in compact heat exchanger, *Experimental Thermal Fluid Sci.* **2**, 100–106 (1989).
4. S. S. Lue, H. Z. Huang and W. Q. Tao, Experimental study on heat transfer and pressure drop characteristics in developing region for arrays of obliquely positioned plates of nonuniform length, *Experimental Thermal Fluid Sci.* **7**, 30–38 (1993).
5. H. Z. Huang and W. Q. Tao, An experimental study on heat/mass transfer and pressure drop characteristics for arrays of nonuniform plate length positioned obliquely to the flow direction, *ASME J. Heat Transfer* **115**, 568–575 (1993).

6. E. M. Sparrow, B. R. Baliga and S. V. Patankar, Heat transfer and fluid flow analysis of interrupted wall channel, with application to heat exchanger, *ASME J. Heat Transfer* **99,** 4–11 (1977).
7. E. M. Sparrow and C. H. Liu, Heat transfer, pressure drop, and performance relationships for in-line, staggered, and continues plate heat exchanger, *Int. J. Heat Mass Transfer*, **22,** 1613–1625 (1979).
8. S. V. Patankar, C. H. Liu and E. M. Sparrow, Fully developed flow and heat transfer in ducts having streamwise-periodic variation of cross-sectional area, *ASME J. Heat Transfer* **99,** 180–186 (1977).
9. S. V. Patankar and C. Prakash, An analysis of the effect of the plate thickness on laminar flow and heat transfer in interrupted-plate passages, *Int. J. Heat Mass Transfer* **24,** 1801–1810 (1981).
10. Y. Asako and M. Faghri, Heat transfer and fluid flow analysis for an array of interrupted plates, positioned obliquely to the flow direction, *Proceedings of the Eighth International Heat Transfer Conference*, San Francisco, CA, Vol. 2, pp. 421–427 (1986).
11. K. Pang, W. Q. Tao and H. H. Zhang, Numerical analysis of fully developed fluid flow and heat transfer for arrays of interrupted plates positioned convergently-divergently along the flow direction, *Numer. Heat Transfer* **18,** (part A) 309–342 (1990).
12. P. R. Eiseman, A multi-surface method of coordinate generation, *J. Comput. Phys.* **33,** 118–150 (1979).
13. P. R. Eiseman, Coordinate generation with precise control over mesh properties, *J. Comput. Phys.* **47,** 331–351 (1982).
14. P. R. Eiseman, Grid generation for fluid mechanics computations, *A. Rev. Fluid Mech.* **17,** 487–522.
15. W. Shyy, A general coordinate system for computing transport phenomena, *Proceedings of the Eighth International Heat Transfer Conference*, San Francisco, CA, Vol. 2, pp. 397–401 (1986).
16. W. Q. Tao, *Numerical Heat Transfer*. Xi'an Jiaotong University Press, Xi'an, China (1988).
17. R. S. Amano, A Numerical study of laminar and turbulent heat transfer in a periodically corrugated wall channel, *ASME J. Heat Transfer* **107,** 564–569 (1985).
18. R. C. Xin and W. Q. Tao, Numerical prediction of laminar flow and heat transfer in wavy channels of uniform cross-sectional area, *Numer. Heat Transfer* **14,** 465–481 (1988).